Liver injuries in frontal crash situations: A coupled numerical-experimental approach

Pj Arnoux, T. Serre, N. Cheynel, L. Thollon, M. Behr, P. Baque, C. Brunet

Liver injuries in frontal crash situations
A coupled numerical – experimental approach

P.J. ARNOUX[1], T. SERRE[1], N. CHEYNEL[2], L. THOLLON[1], M. BEHR[1], P. BAQUE[1], C. BRUNET[1, 3].

[1] Laboratoire de Biomécanique Appliquée, UMRT 24 Faculté de Médecine - INRETS, Université de la Méditerranée, Marseille, France.
[2] Service de chirurgie digestive, thoracique et cancérologique, C.H.U. de Dijon, hôpital du Bocage - 2, Bd. Maréchal de Lattre de Tassigny – BP 77908 – 21079 Dijon cedex.
[3] Service de Chirurgie générale, digestive et endocrinienne - hôpital Nord, chemin des Bourrelly, 13915, Marseille
Corresponding author: pierre-jean.arnoux@inrets.fr

Abstract

From clinical knowledge, it has been established that hepatic traumas frequently lead to lethal injuries. In frontal or lateral crash situations, these injuries can be induced by pure deceleration effects or blunt trauma due to belt or steering wheel impact. Concerning the liver under frontal decelerations, how could one investigate organ behaviour leading to the injury mechanisms? This work couples experimental organ decelerations measurements (with 19 tests on cadaver trunks) and finite element simulation, provides a first analysis of the liver behaviour within the abdomen. It shows the influence of the liver attachment system that leads to liver trauma and also torsion effects between the two lobes of the liver. Injury mechanisms were evaluated through the four phases of the liver kinematics under frontal impact: (1) postero-anterior translation, (2) compression and sagittal rotation, (3) rotation in the transverse plane and (4) relaxation.

Keywords

Liver biomechanics, Finite element modelling, Cadaver experimentation, frontal deceleration

INTRODUCTION

Motor vehicle crashes are responsible of a large number of serious life threatening injuries. NHTSA estimates the number of serious crash injuries occurring each year in the USA at 70000 Brain injuries, 4400 Neck and spinal cords injuries, 80000 chest and abdominal injuries (heart, lungs, spleen, liver and kidneys), 18000 Hip and pelvic injuries, 35000 leg, ankle and foot injuries [1]. If the liver is not the most frequently injured organ, its shape, its locations and consistence (composed of a high percentage of blood) can lead to very severe traumas with high lethal risk [2]. Liver injuries might be attributed to deceleration effects or penetrations in the abdomen in the crash direction. In most of cases, the combination of these two mechanisms is involved. For penetrations mechanisms, the liver is most frequently injured after a contact with car components in front of the passenger (such as the steering assembly and the instrument panel) [3]. 2 point restraint belts (the driver wearing only the shoulder strap) were most likely to produce liver injuries in low severity frontal collisions when the force direction is 1 to 2 o'clock against the vehicle main axis [4, 5]. Therefore, the impact direction could be a gravity factor in side impact situations [4,5]. From clinical observations [2, 6-9], liver injuries could be summarized by a laceration along the falciform ligaments leading to the spreading of the two lobes, with a rupture risk for the right hepatic vein. At high deceleration levels, the posterior attachments of the liver can be broken, especially the inferior vena cava. Lastly in the case of penetration in the abdomen, a liver failure at the hepatic median vein can be induced.

In order to identify injury mechanisms involved and to evaluate abdomen tolerance to impact, many experimental studies were performed (on living animals and on human cadavers). Walfisch [10], by dropping cadavers from two different heights, revealed a link between velocity and compression force For Nusholtz [11] the velocity seems to

significantly affect the liver motion; above the injury threshold no correlation was found between injury severity and velocity level. Kroell et al. [12] determined that for frontal thoracic impacts, the normalized compression was a factor significantly related to injury severity, and the velocity was implicated as a primary factor in the pathogenesis of impact trauma. Using animal experimentations in side impacts, Klaus [13] underlined severe liver injuries in 90° side impact situations. Rouhana [14] showed a correlation between injury severity and applied compression and velocity. Viano [15] defined blunt lateral impact corridors for various velocities (from 4.5 to 9.4 m/s) commonly used for dummy design and showed a correlation between maximum viscous response and abdomen injury risk. Viano [16] showed that low stiffness armrest limits the abdomen (and liver) injuries on pigs in side impacts. Talantikite [17], performing isolated trunk side impacts, proposed a tolerance level of 500 N for the liver and three tolerance levels for the abdomen (60mm deflexion, 4400 N force and 1.98m/s viscosity criteria). All these studies tried to identify injury typology, to define injury tolerance criteria and to evaluate safety systems.

In order to evaluate the abdominal injury mechanisms observed clinically (chronology of liver deformations and kinematics regarding other abdominal structures), we used a coupled numerical/experimental approach to simulate belted and unbelted trunk decelerations. The results lead to evaluating global liver behaviour in the abdominal cavity and the possible induced injuries. If experimental tests alone were not sufficient to provide a good estimation of the liver behaviour and kinematics, by coupling finite element simulation, it was then possible to identify a four phase behaviour of the liver kinematics which could explain the hepatic veins avulsions encountered in real life impacts.

In this paper, an overview of the model definition up to existing validation data is proposed. Then experimental tests performed in the laboratory are reported and simulated

in order to evaluate our model capability and improve our knowledge on liver behaviour in such dynamic loading cases.

MATERIALS and METHODS

Overview of HUMOS model, design and validation

General Model Overview: The HUMOS1 model [18] is the result of an EU BRITE-EURAM project which aimed at developing a 3D finite element model of the human body in driving position and validating using test results in the vehicle crash environment. The first step of the model development process was to select a cadaver close to the 50th percentile European male. The subject was then placed in a car cockpit in driving position and frozen for slicing purposes [19, 20]. Serial sections were performed and digitized in order to produce anatomical data. Organ, muscle and bone contours were identified by anatomists on each section. The contours were processed to create a 3D reconstruction of the human body. The model is made of approximately 50,000 elements and includes descriptions of all compact and spongious bones, ligaments, muscles and tendons, skin, abdominal and thoracic viscera, and intracranial contents (cf. figure 1).

'[Insert Figure 1]'

Physical properties of the different tissues in the body were based on literature data [21-29], and specific experiments were conducted for the HUMOS project. In the model, trabecular and cortical bones were assumed as elastoplastic materials. Soft tissues such as ligaments, tendons, passive muscles, and organs were considered as viscoelastic or elastic materials. Finally, skin and cartilage were assumed to be elastic. Modelling of muscles was performed in two steps. First, volumetric shapes of muscles were generated using solid elements in order to take into account the damping mechanical properties of passive muscles at impact. Secondly, the lines of action for each muscle were modelled as springs. Therefore, a careful attention was paid to the interface definition between each

4

component of the model. Interfaces were modelled to provide for both adhesive properties and sliding friction between moving parts.

Trunk modelling: In the abdomen, the stomach is a continuous mesh including duodenum and pancreas, leading to a peritoneal-retroperitoneal separation which does not strictly correspond to reality. The liver, spleen and kidneys are described as separated entities. Lastly the intestines (small intestine & colon) were gathered in one same part with a continuous mesh and called "Abdominal bag". For the thorax, heart and lungs were modelled and linked together with a continuous connective mesh to fill in remaining gaps in the model. These components were modelled using typical brick elements with Boltzmann or Kelvin Voigt viscoelastic laws [48, 49]. Hard tissues i.e. pelvis, sacrum, spine, clavicle, sternum, scapula and rib bones were described as shell elements for compact bones and solid elements for spongious bones and modelled with an Elastoplastic Johnson cook behaviour law. Ribcage and pelvis cartilage were modelled using elastic shell and solid elements. The "flesh" tissue -skin (shell), muscles (solids) and connective flesh (solids used to fill gap in the model)- was assumed to follow a viscoelastic (Boltzmann & Pointing Thomson) behaviour law. An overview of the main parameters for internal organs and bone components is provided in tables 1, 2 and 3.

'[Insert Table 1, 2 & 3 about here]'

As it was difficult to investigate tissues tribology, according to anatomical considerations, we assumed two different situations in order to describe tissue interactions: Adhesive and sliding properties. These situations can be obtained through three modelling choices:

- The continuous mesh used for stomach, abdominal bag or thorax segment was used to allow interactions between the different components,

- A set of springs (with a 60 to 100N/mm stiffness) was also used for organ attachments (modelling organ ligaments) or to describe adhesive properties between organs and

membranes. It mainly concerned the peritoneal membrane to intestine and liver to spleen attachments (see illustration on figure 2).

- Typical Coulomb friction interfaces with frictional coefficient of 0.1 were used to ensure contact or adhesive properties between the different components of the abdomen and thorax segment (more than 120 interfaces were used)). Note that specific tied interfaces (which consist in kinematics conditions between the two objects) were used to complete attachment of the different organs (see illustration figure 2), especially between intestine and peritoneal membranes, stomach and liver, and liver and peritoneal membranes.

'[Insert Figure 2 about here]'

Validation of the HUMOS model was performed in incremental steps. First, material properties of isolated elements (i.e. cortical bone, trabecular bone, ligament, functional spinal unit, etc.) were evaluated individually on the basis of traction, compression, shearing and bending tests. As behaviour law required parameters which didn't match with available experimental data, optimisation procedures were performed on the difference between experimental and simulated recorded data (usually stress versus strain) in order to fit these parameters using NLPQL methods on Radioss Dss optimisation tool [51]. Next, validation was performed on sub-segments (i.e. head-neck, thorax, upper extremity, etc.) by comparison to experimental data during simulated frontal, lateral and oblique impacts. Finally, the whole model was validated with a sled test performed for the HUMOS project. For the specific case of liver, the model parameters were optimized on the base of quasi-static compression tests [35, 50] and reported in table 3. An overview of the trunk model validation is reported in table 3. Note that more details about model definition and validation procedure were reported in references [18; 25; 26].

'[Insert Table 4 about here]'

Concerning the abdomen, the validation procedure (dealing with liver injuries) focused on abdominal impact tests reported by Viano [15] and Cavanaugh [30]. In Cavanaugh's

study, subjects were seated with their back set vertical, arms along the body, and were suspended by a cable (passing under the armpits) which was released just prior to impact. The linear impactor is horizontal, with its axis centred on L3. The impacting device is a 25 mm wide and 400 mm long cylinder (simulating a steering wheel ring). Two sets of experiments were performed with different velocities and impactor masses ([6.9 m/s, 31.4 kg] and [9.4 m/s, 63.6 kg]). For these tests the validation was computed on force and deflexion on the impactor (see illustration on figure 3). Oblique Impact test are based on Viano's experimental study [15]. For these tests, the impacting surface is circular, 150 mm in diameter, with a 23.4 kg mass and an initial velocities of 4.8, 6.8 and 9.4 m/s. The impact is centred on the thorax with a 30° angle. The impact is delivered at the level of the xiphoid process, 15 cm under the centre of the sternum and validation performed on force versus time and deflexion versus time curves (see figure 4).

'[Insert Figure 3&4 about here]'

Experimental Trunk deceleration tests. In order to investigate liver behaviour in the abdomen during a frontal deceleration, experimental free-fall tests using cadaver's trunks were performed. Trunks from 6 human cadavers (59, 69, 78, 85-year-old men and 2 women aged 81 and 82) were tested. The cadavers (obtained from the pathology department of the University of Mediterranée – Medicine Faculty of Marseilles) were treated with Winckler solution [31] to ensure proper preservation of soft tissues and then held at +3°C until testing. Prior to testing, the trunks were thawed to room temperature, sensors were inserted; and X-rays performed to check bone integrity and sensors orientations. The trunk was dissected by removing upper limbs, head and neck segment, lower limbs, the greater pelvis and the lower abdomen viscera. On the abdominal segment only the colon was kept. From an anatomical point of view, the liver attachments are active on its proximal and rear parts. Therefore, greater pelvis and lower abdominal

viscera were removed as we considered they do not have a mechanical contribution to the behaviour of the whole structure. Trunks were instrumented using 2D and 3D ENTRAN accelerometers (±25g acquisition range, recorded at 10Khz and sampled at 1kHz with a specific conditioning in order to keep water tightness during experiments). 3D accelerometers were fixed on the anterior part of the manubrium sternum and 2D accelerometers on the anterior face of the L1 lumbar spine. Due to the size of sensors it was only possible to use 2D sensors on the vena cava and the left and right lobes of the liver. The liver accelerometers were inserted at the geometrical centre of each lobe using a surgical technique with an insertion direction which was initially perpendicular to the loading axes. The vena cava accelerometer was inserted and then fixed in the vessel using an injected silicone gel. All sensors were inserted in order to have one orientation in the direction of loading and the second one in the lateral medial direction. In order to validate the sensors orientation, during the acceleration phase of the trunk (prior to impact), the acceleration recorded on sensors was compared to the theoretical 1G acceleration (free fall). In order to avoid creating air-filled voids in the abdominal cavity, once sensors were inserted, the abdominal cavity was closed, sutured and then packed in an hermetic bag. The trunk was then belted to the free fall system in order to have the anatomical anterior posterior axes in the impact direction. The free fall system is a vertical mobile which can be released at heights varying from 1 to 4m (cf. figure 5). At the end of the free fall, a braking system stops the mobile set on the same distance whatever the initial velocity. Each trunk was tested with three different sets of velocities (~4m/s, ~6m/s and ~8m/s). All tests were filmed with high-speed video cameras (1000 frames/second) in the frontal view. Accelerations were recorded with a 10 kHz sample frequency. For each test the trunk was belted with a car lateral belt system at the lower sternum and the umbilical regions. One additional test was performed by replacing the belt with a rigid plate. A total of 19 tests were performed.

Numerical Trunk deceleration simulation: To reproduce the same experimental conditions, head neck segment, lower limbs segments (including pelvis), upper limbs segments (up to shoulder connective flesh) were removed from the initial HUMOS model. For the lower abdomen the mesh of the intestine ("abdominal bag") was cut in order to keep the colon as it was performed experimentally. The model instrumentation was obtained using cubic rigid bodies fixed on tissue neighbouring nodes. Each cubic rigid body was obtained as defined with 9 nodes (8 for the brick and 1 for the centre), with a 10mm characteristic dimension and a 10g mass. The sensor orientation was defined using typical skew systems linked to the rigid body (cf. figure 6) with the anatomists already involved in the experiments, and adapted to the Humos1 liver.

The first numerical simulation deals with the case of a trunk fixed to a rigid plate in pure deceleration (cf. figure 7). The test was obtained in two steps:

- Trunk positioning: the rigid wall was fixed (both in rotations and translations) whereas a constant velocity was applied (during 10ms) on different spine elements in order to obtain a homogenous support of the trunk in front of the rigid wall.

- Deceleration test: the rigid wall boundary condition consisted of fixing rotation and translation except for the z axes (in the direction of deceleration). All nodes of the model were defined with an initial velocity of 7.7m/s (velocity recorded just before deceleration). Then the deceleration curve recorded experimentally (test n°13) on the support was applied to the rigid wall.

The second set of numerical experiments consists in using similar belts as those used in our experiments (cf. figure 7). The rigid wall is now below the trunk. Belts were set in

similar positions as experimental ones (upper sternum and lower ribcage). Interfaces between belt and trunk were defined, except for the shoulder connective flesh. A velocity of 6.3m/s was set to all nodes of the model and the experimental acceleration of the support was applied to the wall.

'[Insert Figure 7 about here]'

RESULTS ANALYSIS

Experimental cadaver tests

The acceleration curves obtained from these experiments were analysed in two ways. A first focus was performed on 1D accelerations in the initial postero anterior and latero medial direction (cf. figure 8).

'[Insert Figure 8 about here]'

From these curves, it was possible to evaluate the different phases of the test:

- During the free fall phase (from A to B on figure 9), the acceleration was first constant and close to 1g (slightly below due to friction of the falling system and possible default in initial sensor orientation) in the postero anterior direction and closed to 0g in the lateral medial direction. From these recorded accelerations it was then possible to evaluate velocity of the system before impact and then check the orientation of each sensor by comparing it to the theoretical acceleration for a free fall.

- The deceleration phase was obtained between the maximum velocity and the zero velocity (from point B to C on figure 9) and showed a time duration ranging from 45 ms to 51 ms according to the initial velocity (from 4.6 to 8.1m/s). During this first phase, no significant time shift was observed between the different sensors(less than 5ms) and seems to show a good global behaviour of the whole structure.

- The rebound phase was associated with the elastic response of the structure up to the system immobilization. We will focus on the period between zero velocities up to the maximal velocity in the rebound (point D on figure 9). During this phase (and compared

to the deceleration phase) some dispersions from each organ were observed on acceleration levels and curvilinear velocity shift durations (shift on the x axis). The differences in acceleration levels can be attributed to the mobility of each organ within the abdomen but also to the rotation of sensors during the deceleration test. If for sensor screwed on bones it was assumed that no significant rotation occurred during the test, it is not the case for liver and surrounding vessels. These rotations could be amplified by strain effects on each organ. For the two different sensors inserted on each lobe of the liver (with the same initial orientation), strong differences were recorded and could be attributed to strain effects between the two lobes. This could be linked with a larger displacement of the left lobe along its curvilinear trajectory as compared to the right lobe. If we focus on maximum acceleration level for each direction, the maximum acceleration seems to be a linear function of the impact velocity with a regression factor ranging from 17 to 22 (s^{-1}) according to the different trunk and sensors used. This relation could be an indicator of potential injury in the abdominal region once damaging impact velocities will be reached.

'[Insert Figure 9 about here]'

Concerning the deceleration and rebound phases, and more specifically the period between maximal and minimal velocity (from B to D), two groups of time durations could be identified: the hard tissues (including L1 and Sternum sensors) and soft tissues (vena cava inferior, left and right liver) for which the time shift depends on the initial impact velocity and can reach 9m/s for high velocity tests. This delay could be linked to inertial effects of the liver (which is a voluminous organ), to strain effects on soft tissues and to differences on material properties between hard and soft tissues. From autopsies performed after experimentation, no hepatic injuries were found. The sensor inclusion was carefully inspected: no variation of position was observed and no additional damage on tissues was observed. X-rays did not reveal any rib failure either.

Finally, for the tests performed, results showed a very strong reproducibility. For the same trunk tested with different velocities, no significant variation on data recorded during the first phase was observed. It seems to show that the liver was not injured during the previous tests. It also means that the sensor orientation was not modified and that the liver goes back to its initial position in the abdomen after the test.

Validation of numerical simulations

In this study, numerical simulations were used at two different levels: Firstly numerical simulation consisted in comparing model response and experiments focusing on the accelerations recorded in the initial loading direction for L1, sternum, right liver and left liver. For both experiments and simulations, data post processing was performed in the same way (same shift on the beginning of the deceleration curve, same sampling at 10 kHz) and started at the deceleration phase. Assuming that the liver model kinematics are relevant with experimental results, the model response (i.e. each acceleration recorded) was relevant with experimental data in terms of time, acceleration amplitude and curve slope for both sets of experiments (cf. figure 10). Time integration on experimental and numerical accelerations was performed to obtain curvilinear velocity (cf. figure 11).

'[Insert Figure 10 & 11 about here]'

From numerical simulation to injury mechanisms

Assuming the model to be validated in the initial loading direction, it is now possible to determine all acceleration components recorded during numerical simulations (cf. figure 12), to compute Von Mises stress curves on bones, pressure levels, strains of organs as well as sensor rotation effects.

Concerning Von Mises stress curves, both deceleration situations studied in this work (rigid plan or belted trunk) showed global flexion effects of the thoracic cage with a time duration close to 120ms. Von Mises amplitude did not change between both tests with

Von Mises level reaching 28MPa (cf. figure 13). Nevertheless, strong differences appear concerning the distribution and amplitude of stress levels on the structure. The rigid plate tests showed high stress levels located on the whole sternum and on the middle components of the costal grid, whereas the belted trunk show low stress levels with an homogenous distribution on the whole structure and only small stress peaks on sternum.

'[Insert Figure 12 & 13 about here]'

As it was reported from experiments, no liver translation was recorded along the trunk axis which is relevant with anatomical considerations about the attachment system of the liver. The liver behaviour first exhibits a global translation in front of the costal grid during the first part of the deceleration curve and then a rotation around the spine (for its posterior part) , limited in the anterior part by the costal grid curvature (cf. figure 14). At the end of the test (i. e. at 120ms), the liver moves back to its initial position. The rotation effects of sensors were recorded and reported on figure 15. From the model analysis, the right liver (which is the most massive lobe), rotation effects up to 40° were observed whereas for the left lobe the rotation only reached 30°. These results confirmed the rotation effects observed with the model and underlined relative deformations between both lobes of the liver. These observations were also confirmed on velocity shifts between right and left lobes at the beginning and the end of the deceleration phases.

'[Insert Figure 14 & 15 about here]'

DISCUSSION

Using an hybrid approach, i.e. coupling experimental data and numerical simulations, it was possible to evaluate abdominal organ behaviour and more specifically liver behaviour under frontal dynamic sub injury deceleration tests.

On experimental results

Experimental data on cadaver testing under dynamic loading are usually recorded by screwing or sticking accelerometers on bones. Few attempts have been performed to instrument soft tissue structures. This first set of experiments showed that it was possible to perform such experimentations and open large prospects of experimentation concerning thoracic and abdominal organ behaviour under crash situations. Even though results should be carefully analysed and can not be directly used to postulate on injury mechanisms or injury thresholds. They need to be coupled with numerical simulation in order to provide a more exhaustive analysis of the problem.

The way sensors were used (set perpendicular to the loading axis and followed by silicon inclusion) showed good efficiency and did not induce any orientation or initial position variations, as observed in sets of experiments performed with one same instrumented trunk. If the sensors orientation before and after each experiment was checked with acceleration curves and X-rays measurements, some improvements should be performed concerning the X-rays identification of initial orientation, by inserting specific markers on the sensors. As we were concerned about avoiding tissue damage during experiments, small-sized 2D accelerometers were used. But it limits the possibilities of analysing experimental results. Even if the ratio between liver and sensors density is around 2.5, the liver global mass is around 1.6Kg compared to 20g for the two 3D sensors. This point leads us to assume that sensors inertial effects can be negligible regarding whole liver inertial effects. Further experiments should involve small 3D sensors (and new technology sensors [47]) in order to avoid tissue damaging (regarding liver density and water tightness).

The results obtained show a strong reproducibility on the 19 tests performed as well for the general curve shape as for recorded data amplitude and time durations. If these 1D and 2D accelerations can not be directly used to study the structure behaviour, these data were strictly necessary to the model evaluation and validation. Using accelerometer data in

order to evaluate velocities or displacement is a very complex task for which numerical integration can provide strong errors. Moreover, experimental data analysis was based on the different time phases of the phenomena and then used to validate the model response. Amplitude phenomena were only used directly on acceleration data. As experimental results were compared to simulations, they were submitted to the same post-processing procedure as for simulations.

The differences in terms of time duration between the different sensors during the deceleration phase could be qualitatively analysed. These results seem to indicate two phase behaviour: (1) global kinematics of the internal organs during the first part of the trunk deceleration, (2) increasing time shift (with impact velocity) between hard tissues (L1 and sternum) and soft tissues structures (left lobe, right lobe and vena cava inferior). These results show significant differences concerning kinematics of the liver itself and its surrounding structures. Therefore, with a high velocity level, differences in time duration (up to 6ms) appear between L1, right and left liver. This dispersion is significant and may be considered as an indication of the global kinematics of the liver regarding L1, but also strain effects between left and right liver lobes. It also shows the contribution of the vena cava inferior in the mechanical attachment of the structure. Lastly, it seems that the liver morphology (i.e. anterior spreading and posterior spreading) could have an influence on results, but require more experiments to be discussed in detail.

About numerical simulation: model evaluation and hybrid analysis

The Humos model put in the same conditions as the experiments show relevant results (assuming the sensor kinematics are relevant with experimental ones) with those obtained for both types of experiments (belted trunk and trunk fixed on a rigid plate). Humos being in seating position, its spine curvature is different from those of experiments, due to standing position of the PMHS. Consequently the model quality response could be improved by setting the model in standing position prior to the test. Regarding model

sensitivity, it has been shown that model mass, model geometry, behaviour laws and obviously mesh size can induce significative variations in the model responses especially when model is used to investigate high speed loading and failure domain [18, 25, and 26]. As in this study, we focus on global liver behaviour and kinematics; the question of model sensitivity was estimated regarding model behaviour. Complementary tests were performed to investigate friction coefficient influence on liver related interfaces by setting all friction coefficient to 0,2 and 0,4. The resultant acceleration exhibit some variations in amplitude but not in phenomena described (cf. figure 16). These variations were in the same magnitude as biological variability regarding experimental tests performed. Consequently, they are not assumed to modify significantly model kinematics and results obtained in this work.

'[Insert Figure 16 about here]'

Mesh size influence on structure behaviour was also evaluated with a very fine mesh (mean element length of 1mm) for quasistatic compressive tests on isolated liver. The results obtained showed global equivalent response between the two meshes concerning the elastic phase of mechanical behaviour (cf. figure 2). As this study doesn't focus on flexion modes and local stress and strain level on liver structures these differences were assumed to not significantly influence the results obtained. Nevertheless, improving model mesh quality with smaller elements length would be an important evolution of the model especially for the accuracy of structure mechanical behaviour at failure level.

'[Insert Figure 17 about here]'

Adding to the typical validation procedure, these tests were used to improve model robustness by performing corrections in interface definitions. For all interfaces of abdominal segment, intersections were suppressed (regarding liver and neighbouring organs and structures) through normal locally translation of intersected nodes.

Penetrations were corrected by diminution of gap (with no gap under 0.8mm) or local translation of nodes. Lastly, each interface which gathered slave and master components was replaced by two symmetrical interfaces. The analysis of numerical simulations shows a more complex liver behaviour in the abdomen as the initial assumption of anterior posterior translations issued from the kinematics energy evaluation performed by clinical studies [6-8]. From the current experimental and numerical results, the liver behaviour could be divided into four main phases (cf. figure 18):

- 1. During the first part of the deceleration phase, the liver exhibits a postero-anterior global translation up to the contact with the ribcage.

- 2. Then, induced by inertial effects of liver and flexion of the ribcage, an anterior posterior compression of the liver was observed. This phenomenon leads to a transverse strain effect and a sagittal rotation of the liver.

- 3. The rotation phase was observed in the transverse plane. This rotation is induced and limited by ribs curvature in the frontal part and by the spine in the posterior part of the trunk.

- 4. Finally, in the case of sub injury impact tests, we observed a global relaxation in which the structure moves back to its initial position.

'[Insert Figure 18 about here]'

Adding to the strain effects between the right and left lobes of the liver, this work shows that the posterior attachments of hepatic organs are essential. This conclusion led to improve the model definition by including a segment of vena cava inferior and its insertions in the liver. New simulations performed with this more accurate description of posterior attachment structure of liver confirmed the four phase liver behaviour especially with rotation around vena cava inferior (cf. figure 19). It also led to a first description of possible avulsion mechanism on the vena cava inferior (cf. figure 19). Such simulations need to take into account more accurately mechanical properties of tissues [32-39]

especially with failure properties of liver and veins to describe macroscopic liver failure around the falciform ligaments and hepatics veins.

'[Insert Figure 19 about here]'

CONCLUSION

The main objective of this work was to show how, coupling a finite element model of the trunk (extracted from the HUMOS Model) and an experimental approach, it was possible to provide analysis of the liver behaviour during a frontal impact. From an experimental point of view this work showed that it was possible to instrument soft tissues structures of hepatic organs to evaluate acceleration levels. Further works will focus on the improvement of this technique by including new 3D accelerometers and if possible rotation sensors. Then these experimental data were confirmed by numerical simulation and showed the model ability to describe such behaviour. Assuming the model as validated, numerical results analysis exhibited a four phase behaviour including deceleration, compression, rotation and relaxation of the liver, up to the influence of the restraint system in terms of Von Mises stress distribution during the test. Lastly the specificity of the liver behaviour provides research improvement ways which concern vena cava inferior and falciform ligament descriptions in order to evaluate injury risks for hepatic organs. The last results obtained confirmed these trends, especially with the hepatic vein avulsion. However, this model has limitations in terms of mesh refinement and descriptions of damage behaviour laws which limits the model validity to accurately describe failure processes. These first results have to be improved with further developments, including implementation of damage and failure properties of biological tissues and a large sensitivity study including different liver morphotypes in order to define a risk corridor for these ultimate levels.

Lastly, liver injuries can not only be attributed to pure frontal deceleration effects. In many real life situations like car lateral impacts, decelerations are coupled with penetration effects. The results obtained in the work need to be extended to such situations.

ACKNOWLEDGMENTS

REFERENCES

[1] CIREN, 2000, NHTSA CIREN Program Report

[2] Yogonandan n., Pintar F. A., Maltese M.R., 2001, Biomechanics of abdominal injuries, *Critical Reviews in Biomedical Engineering,* 29(2), pp. 173-246

[3] Lee J.B., Yang K.H., 2002 Abdominal injury patterns in motor vehicle accidents : a survey of the NASS database from 1993 to 1997, *Traffic Injury Prevention,* Vol. 3, N°3, pp. 241-246

[4] Augenstein JS, Perdeck E, Bowen J, Stratton J, Horton T, Singer M, Digges KH., Steps JH. Injuries to Restrained Occupants in Far-Side Crashes. *44th Annual Proceedings, Association for the Advancement of Automotive Medicine*, October 2000, p. 57.

[5] Augenstein JS, Perdeck E, Bowen J, Stratton J., Horton T, Singer M, Digges KH, Malliaris AC, Steps J. Dummy Measurement of Chest Injuries Induced by Two-Point Shoulder Belts. *44th Annual Proceedings, Association for the Advancement of Automotive Medicine*, October, 2000, p. 1.

[6] Chevalier J.M., Jost J.L., Vayre P., (1991), Traumatismes du foie – Lésions anatomiques, essai de classification, *Journal de chirurgie,* Vol. 128, N°12, pp. 509-510

[7] Létoublon C., Castaing D., (1996), Les traumatismes fermés du foie, *98ème congrès français de chirurgie*, pp. 20- 58

[8] Contoslavos DL, Laposata E.A. (1992), Sagittal liver transection –an injury from improperly worn shoulder harness seatbelts : a report of two cases, *J. Trauma*, 33, (4), 637-640.

[9] Brunet C., Sielezneff I., Thomas P., Thirion X., Sastre B., Farisse J. (1994), Treatment of hepatic trauma with perihepatic mesh: 35 cases. *The Journal of Trauma, 37(2):200-203*

[10] Walfisch G., Fayon A., Tarrière C. & al. (1980), Designing of a dummy's abdomen for detecting injuries in side impact collisions. *Fifty international IRCOBI Conference Proceedings,* pp. 149-164

[11] Nusholtz G.S., Melvin J.W., Mueller G. & al., (1980), Thoracoabdominal response and injury. *24th Stapp Car Crash Conference Proceedings, pp. 187-228*

[12] Kroell C.K., Pope M.E., Viano D.C, (1981), Interrelationship of velocity and chest compression in blunt thoracic impact, *25th Stapp Car Crash Conference,* SAE 811016, pp 549-579

[13] Klaus G., Kallieris D., (1983), Side impact : a comparison between HSRI, APROD and Hybrid II dummies and cadavers, *27th Stapp Car Crash Conference,* SAE 831630, pp 134

[14] Rouhana S. W., Kroell C.K., (1989), The effect of door topography on abdominal injury in lateral impact, 33th *Stapp Car Crash Conference Proceedings,* n°892433, pp. 227

[15] Viano D.C., (1989), Biomechanical responses and injuries in blunt lateral impact, *SAE Proceedings of the 33th Stapp Car Crash Conference*, pp. 113-142

[16] Viano D.C., Andrzejak D., (1993), Biomechanics of abdominal injuries by armrest loading, *The Journal of Trauma,* vol. 34, N. 1, pp. 105-115

[17] Talantikite Y., Brun Cassan F., Lecoz J.Y., Tarrierre C., (1993), Abdominal protection in side impact injury mechansims and protection criteria, *IRCOBI Conference Proceedings*, pp. 131-144

[18] Behr M., Arnoux P.-J., Serre T., Bidal S., Kang H.S., Thollon L., Cavallero C., Kayvantash K., Brunet C. (2003), A human model for road safety: from geometrical acquisition to model validation with Radioss. *Computer methods in biomechanics and biomedical engineering*, Vol 6 n°4, 2003, pp263-273.

[19] Ghannouchi S, Ghorbel A, Cavallero C, Bonnoit J (1993) Anatomy of the seated position : methodologic approach and initial findings. *Surgical Radiology Anatomy,* Vol. 15, pp. 315-319

[20] Serre, T., Brunet C., Durand F., Bidal S., Ghannouchi S., Behr M., Cavallero C., Bonnoit J., (2002), The seated man : geometry acquisition and 3D reconstruction *Surgical and Radiologic Anatomy Volume24, Issue 6 pp381-386 - Springer-Verlag*

[21] Viano D.C., Lau I., (1983), Role of Impact velocity and chest compression in thoracic injury. *Aviat. Space Environ. Med.,* 54, pp. 16-21

[22] Viano D.C., (1986), Biomechanics of bone and tissue : a review of material properties and failures characteristics, *SAE*, pp 33-63

[23] Yamada H., (1970), Strength of biological materials, *the William and Wilkins Company Baltimore*

[24] Fung Y.C., (1993), Biomechanics: Materials properties of living tissue, *Springer Verlag*.

[25] Arnoux P.J., Kang H.S., Thollon L., Kayvantash K., (2001), *Radioss Humos model guidelines*, Mecalog safety business unit©.

[26] Arnoux P.J., Kang H.S., Kayvantash K., (2001), HUMOS project Deliverable WP5-6, *European 5th framework*, deliverable 6ISA /010710/E1/DA

[27] Dan D., (1999) Caractérisation mécanique du foie humain en situation de choc. *Ph D dissertation*, Université Paris 7

[28] Lizée E, Robin S. et al, Besnault B. and al., (1998), "Development of a 3D Finite Element Model of the Human Body". *42th Stapp Car Crash Conference*, Paper n° 983152.

[29] Lizée E. et al, Song E. et al., (1998), "Finite element model of the human thorax validated in frontal, oblique and lateral impacts : a tool to evaluate new restraint systems". *Proceedings of the International IRCOBI Conference on the biomechanics of impact*

[30] Cavanaugh J.M., Nyquist G.W., Goldberg S.J., King A. I., (1986), Lower abdominal tolerance and response, *SAE*, Paper N° 861878.

[31] Winckler G., (1974), Manuel d'anatomie topographique et fonctionnelle, *Masson Ed.*

[32] Jian, C., & Wang, G. (1991) Biomechanical study of the bile duct system outside the liver. *Bio-Medical Materials & Engineering*, Vol. 1, pp. 105-113.

[33] Liu, Z., & Bilston, L. (2000) On the viscoelastic character of liver tissue: experiments and modelling of the linear behaviour. *Biorheology*, Vol. 37, pp. 191-201.

[34] Liu, Z., & Bilston, L. E. (2002) Large deformation shear properties of liver tissue. *Biorheology*, Vol. 39, pp. 735-742.

[35] Miller, K. (2000) Constitutive modelling of abdominal organs. *Journal of Biomechanics*, Vol. 33, pp. 367-373.

[36] Seki, S., & Iwamoto, H. (1998) Disruptive forces for swine heart, liver, and spleen: Their breaking stresses. *Journal of Trauma-Injury Infection & Critical Care*, Vol. 45, pp. 1079-1083.

[37] Wang, B. C., Wang, G. R., Yan, D. H., & Liu, Y. P. (1992) An experimental study on biomechanical properties of hepatic tissue using a new measuring method. *Bio-Medical Materials & Engineering*, Vol. 2, pp. 133-138.

[38] Koop B.E., Lewis J.L., (2003), A model of fracture testing of soft viscoelastic tissues. *Journal of Biomechanics, Vol. 36, pp. 605-608*

[39] Rubin M.B., Bodner S.R., (2002) A three dimensional nonlinear model for dissipative response of soft tissue, *International Journal of Solids and Structures*, Vol 39, pp. 5081-5099.

[40] Demetropoulos C.K., Yang K.H., Grimm M.J., Khalil T., King A.I, (1998), Mechanical properties of the cadaveric and Hybrid III lumbar spines, *Proceedings of the 42nd STAPP Car Crash Conference*

[41] Kalieris D., Riedl H., (1998), Experimental activity WP3.2, *European 5th framework* HUMOS deliverable 3HEI/981110/T1/DA,

[42] Bouquet R., Ramet M., Bermond F., Cesari D., Thoracic and human pelvis response to impact, *Porceedings of the 14th International technical conference on enhanced safety of vehicles,* pp. 100-109

[43] Kroell, C.K., Schneider, D.C., Nahum, A.M. (1971). Impact tolerance and response of the human thorax. In: Proc. *15th Stapp Car Crash Conference*, pp. 84–134. Paper No. 710851.

[44] Kroell, C.K., Schneider, D.C., Nahum, A.M. (1974). Impact tolerance and response of the human thorax II. In: Proc. *18th Stapp Car Crash Conference*, pp. 383–457. Paper No. 741187.

[45] Nahum A.M., Melvin J., (1985), The biomechanics of trauma, *Appleton century crofts*

[46] Vezin P., (2000), PMHS tests and analysis, HUMOS project Deliverable WP4, *European 5th framework*, deliverable 4INR /000605/T1/DB

[47] Hardy WN, Foster C, Mason M, Yang KH, King AI, Tashman S., (2001) Investigation of head injury mechanisms using neutral density technology and high-speed biplanar X-ray. *Stapp Car Crash Journal*, Vol. 45, pp. 337–368.

[48] Lemaitre J., Chaboche, J.L. (1990), Mechanics of Solids, *Cambridge University Press.*

[49] Christensen, R.M., (1982), Theory of Viscoelasticity. *Academic Press, New York.*

[50] Melvin JW., Stalnaker RL., Roberts VL. (1973), Impact injury mechanisms in abdominal organs, *17th Stapp Car Crash Conference,* Paper 730968

[51] Schittkowski K. (1986): NLPQL: A FORTRAN subroutine solving constrained nonlinear programming problems, *Annals of Operations Research*, Vol. 5, pp. 485-500

List of tables

Parts	K	G_0	G_I	β	ρ (kg/m3)
Organ_Spleen	0.25	0.054	0.04	1	1000
Organ_Intestine	0.001	0.036	0.027	1	1000
Organ_Kidney_L&R	0.166	0.045	0.036	1	1000
Organ_Stomach	0.25	0.054	0.04	1	1000
Organ_Liver	0.166	0.045	0.036	1	1000
Flesh_Abdominal	0.01	0.045	0.036	1	1000

Table 1: Summary of Boltzmann viscoelastic properties of internal organs with K the Bulk modulus, G_0 the Short time shear modulus, G_I the long time shear modulus, β the decay constant and ρ the density [21-29]

Parts	E (Mpa)	ν	ρ (kg/m3)	$η_0$
Muscle_Pelvabdo	0.532	0.43	1000	5
Muscle_Gluteal_L&R	0.532	0.43	1000	5
Flesh_Pelvic	0.532	0.43	900	5
Thoracic & abdominal connective tissue	0.532	0.43	900	5

Table 2: Summary of connective tissue main parameters for Trunk segment using Pointing Thomson behaviour law with E the Younk modulus, ν the Poisson ratio, ρ the density and η

	Compact	Spongious
Young Modulus	9-15 GPa	10-450 MPa
Poisson ratio	0,3	0,3
Yield stress	80-120 MPa	10 MPa
Ultimate stress	110-130 MPa	15 MPa
Hardening (param & coel)	100 MPa, 0,1	100 MPa, 0,1
Ultimate strain	2-3 %	3%

Table 3: Summary of elastoplastic properties of bones [18, 25, 26]

COMPONENT TEST	References
TRUNK	
Lumbar spine: Demetropoulos flexion extension	[40]
Rib: quasi static and dynamic bending	[18,25,41]
Clavicle: Quasi static en dynamic bending	[18,25,41]
Clavicle: Quasi static axial compression	[18,25,41]
WHOLE MODEL TESTS	
TRUNK	
Thorax bouquet frontal impact	[42]
Thorax Kroell frontal impact	[43,44]
Thorax Nahum frontal impact	[45]
Thoarx Lizee lateral impact	[28, 29]
Thorax Talantikite lateral impact	[17]
Thorax Viano oblique impact	[15]
Abdomen Cavanaugh frontal impact	[30]
Abdomen Viano oblique impact	[15]
Pelvis Bouquet lateral impact	[42]
Pelvis Viano lateral impact	[15]
INRET-Bron Frontal sled tests	[18,25,46]

Table 4: Overview of model validation database regarding trunk segment

List of figures
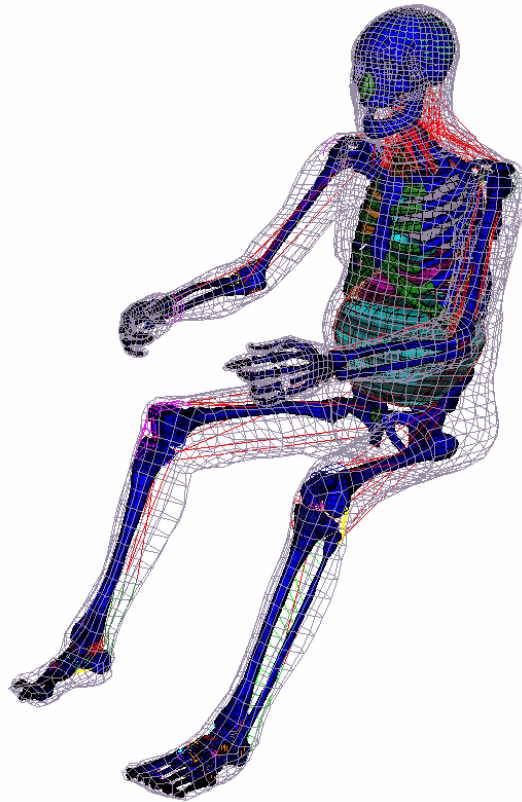
Figure 1: Global overview of the HUMOS model in sitting position
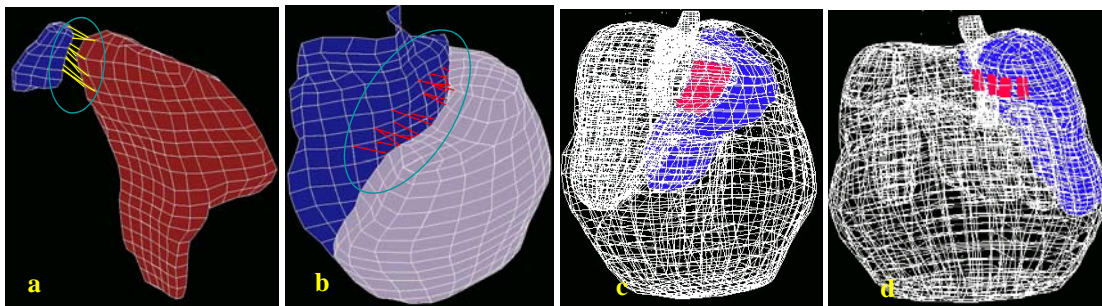
Figure 2: From left to right : **(a)** Spleen stomach attachments (left picture); (**b**) Peritoneal membrane intestine attachments (right picture) to model mesentery, **(c)** Stomach liver attachments ; **(d)** Peritoneal membrane liver attachments
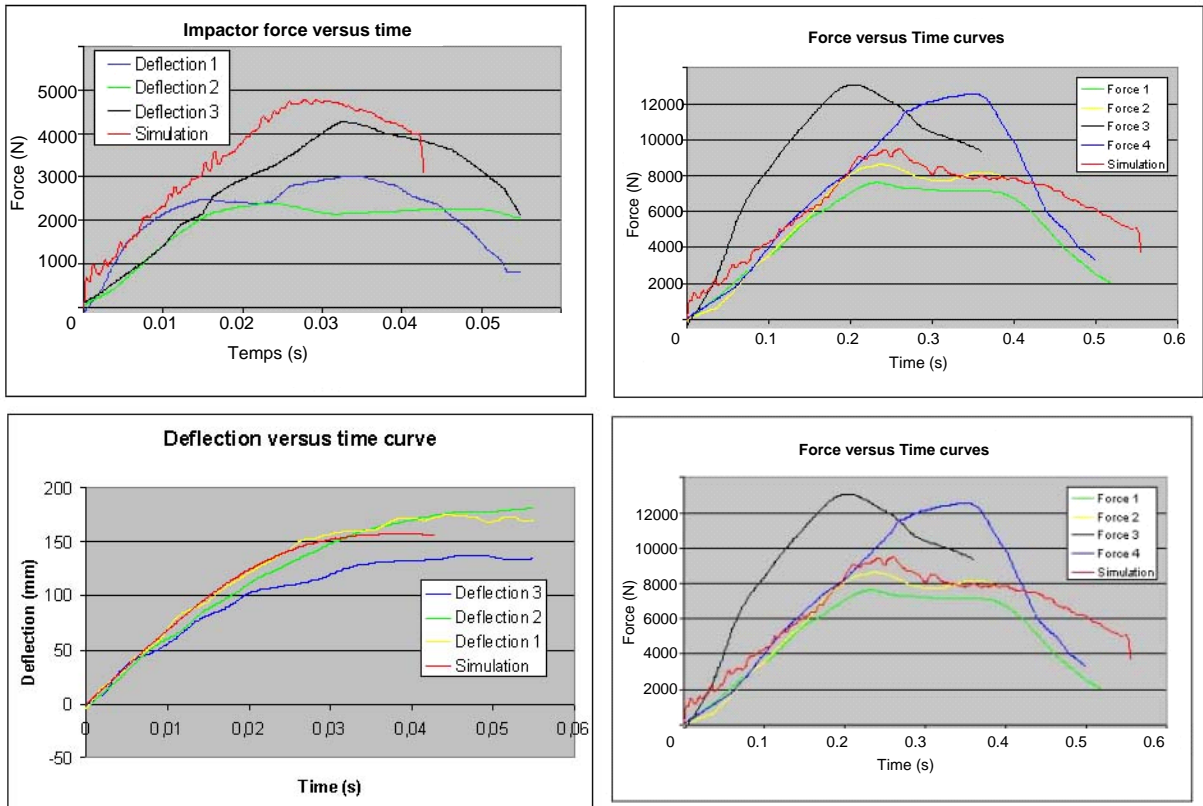
Figure 3: from left to right Cavanaugh 6.9 m/s, 31.4 kg impacts results and 9.4 m/s, 63.6 kg impact results
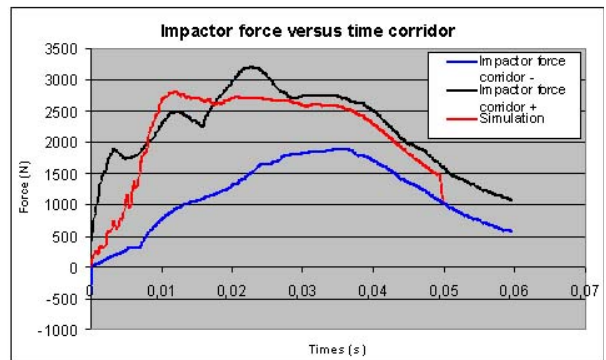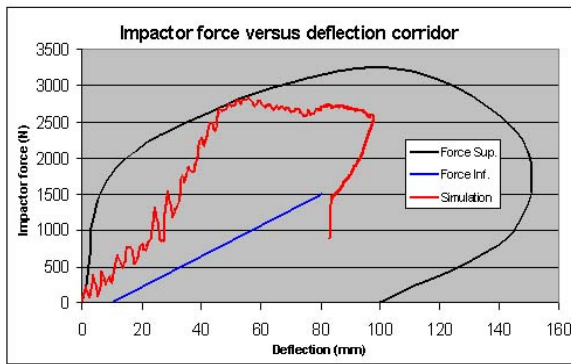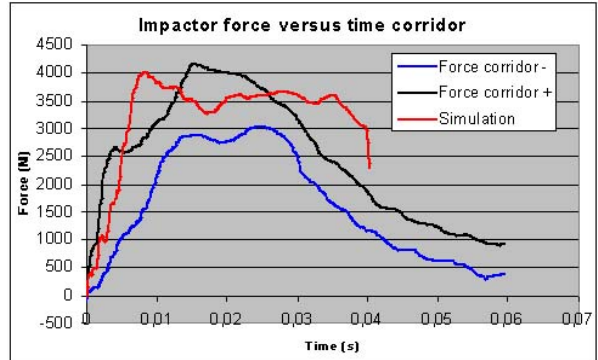
Figure 4.a : Viano 4.8m/s results
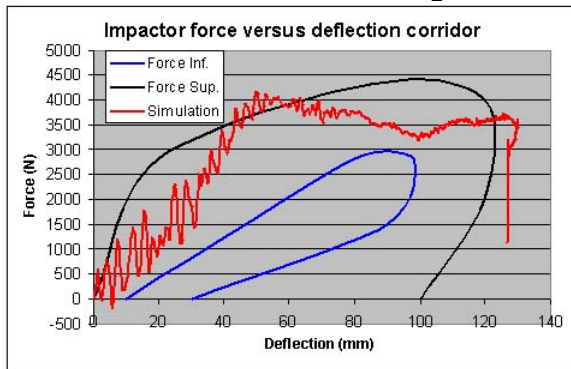
Figure 4.b : Viano 6.8m/s results
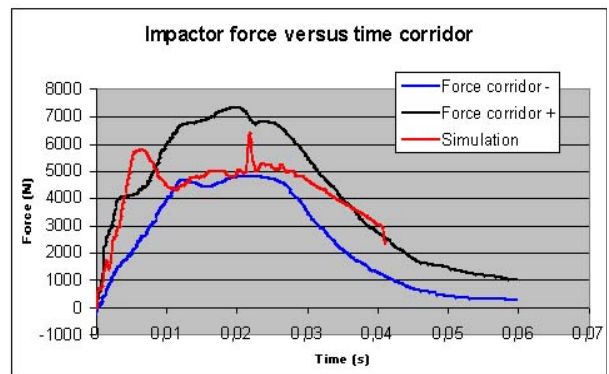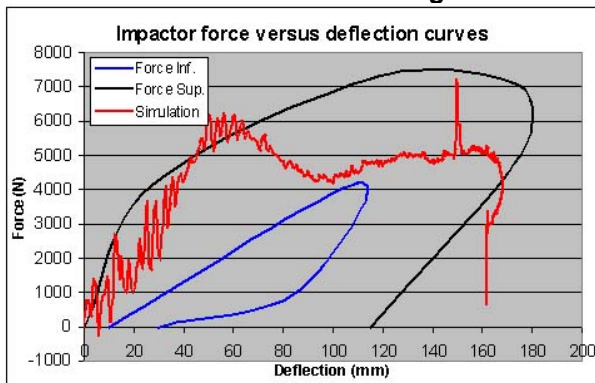
Figure 4.c: Viano 9.4m/s results
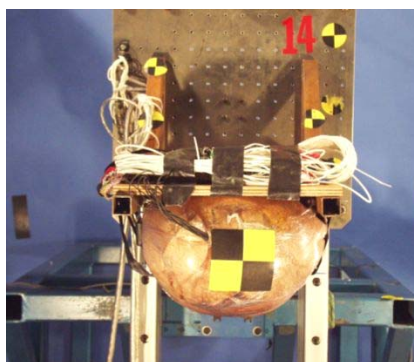
Figure 5: Global view of the experimental set up, frontal view of the belted trunk before the test
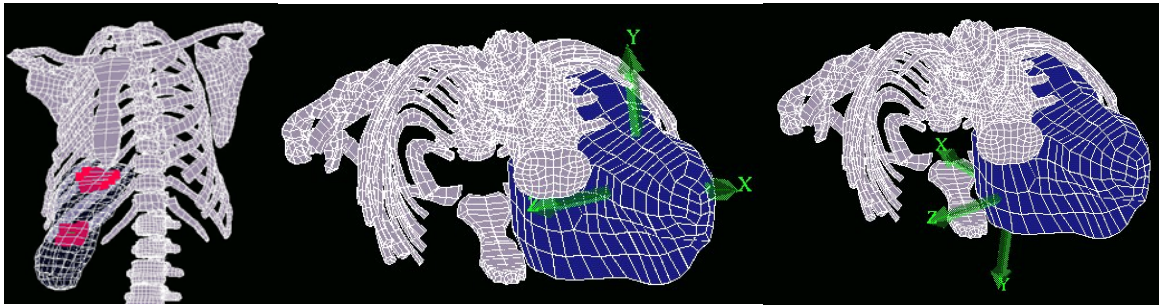
Figure 6: Liver sensors and their corresponding skew systems. On left picture the left liver sensor is reported above and the right one below. On middle picture the left lobe skew is described. On the right picture the right lobe skew is reported.
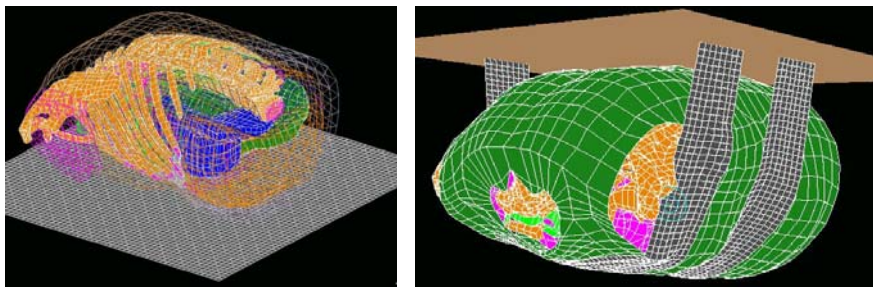
Figure 7: Overview of the two testing conditions (rigid wall and belted trunk)
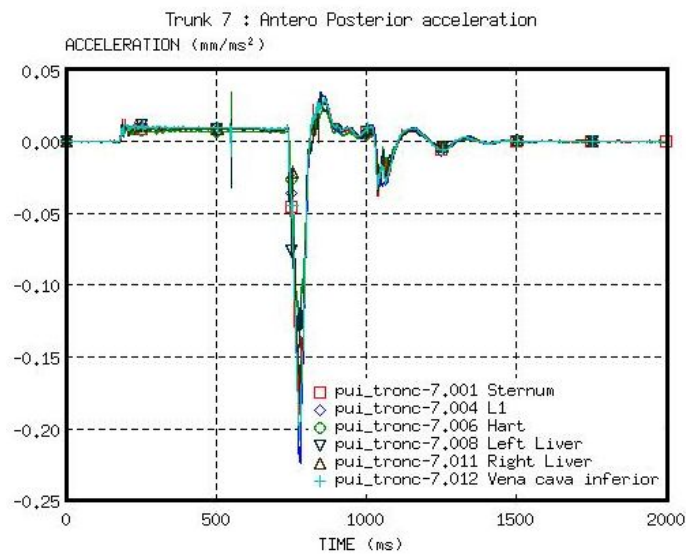
Figure 8: Overview of the unfiltered acceleration curve for the trunk 7 in the antero posterior direction
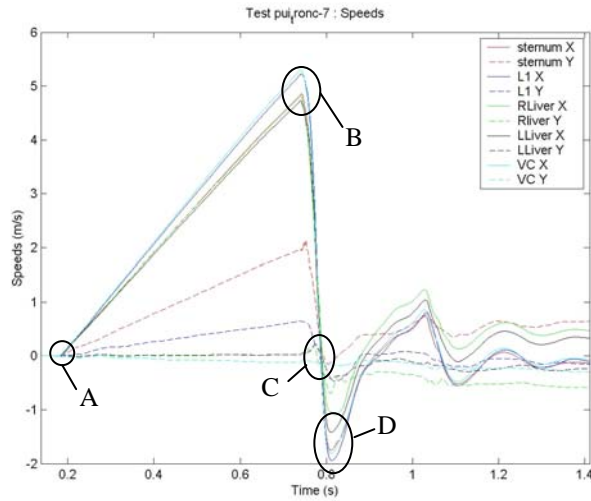
Figure 9 : Trunk 7 curvilinear velocity in antero posterior and latero medial direction by integration of 1D accelerations data. From A to B the acceleration phase of the system, from B to C the deceleration phase of the trunk up to first zero velocity and from C to D and after, the rebound phase with D the maximal velocity in the rebound phase.
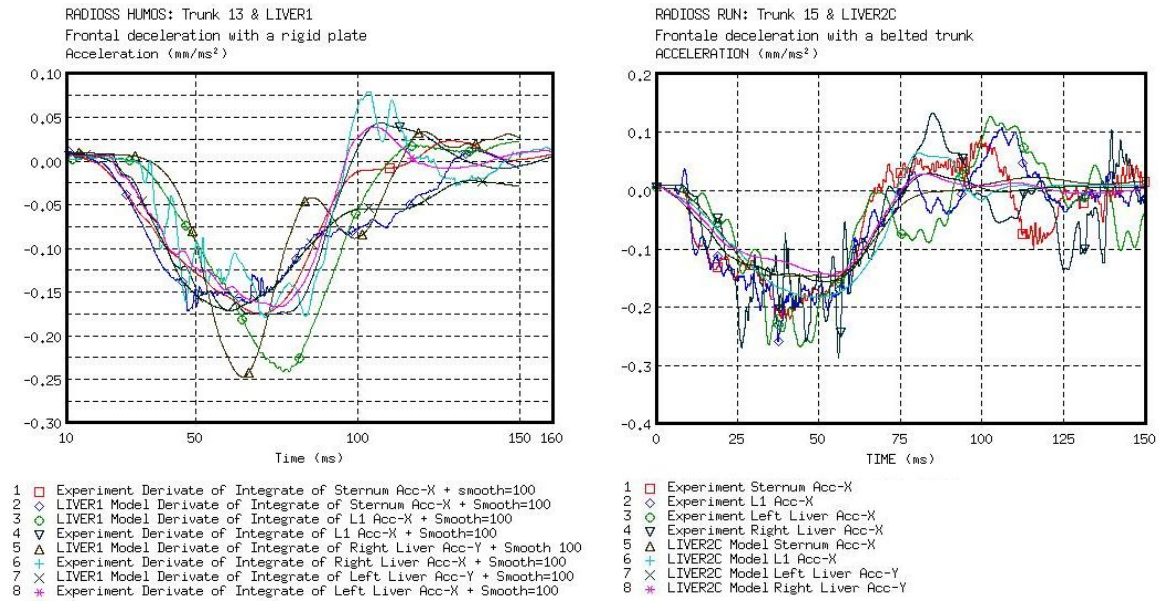
Figure 10: Comparison of experiment and numerical smoothed acceleration versus time curves for Test 13 with trunk on a rigid plate and test 15 for a belted trunk
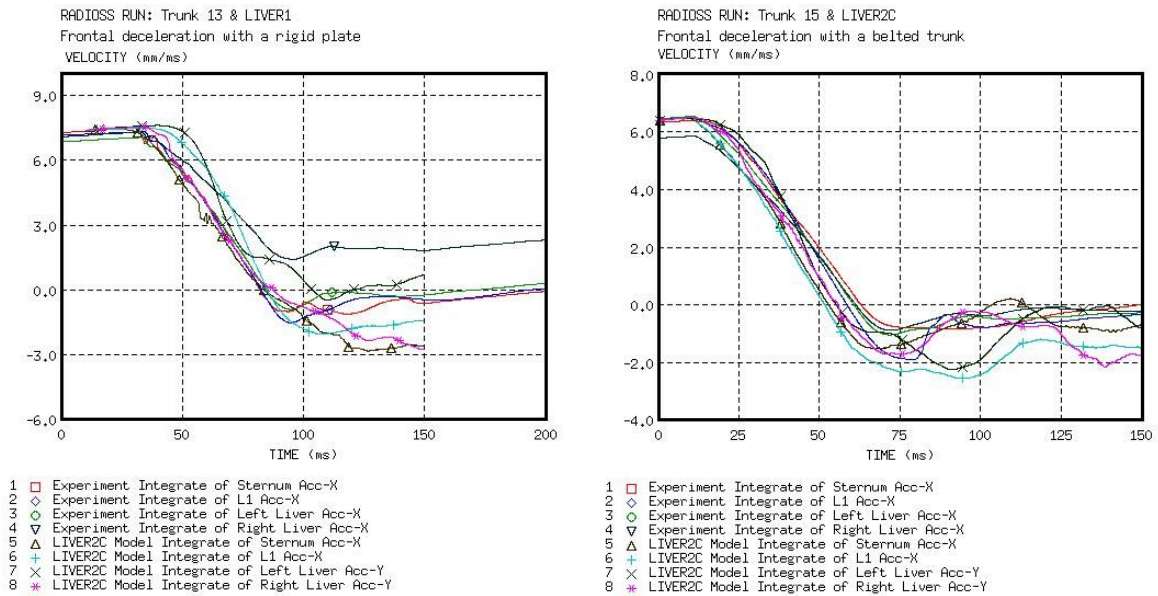
Figure 11: Comparison of experiment and numerical curvilinear velocity (in the initial direction of impact) versus time curves for Test 13 with trunk on a rigid plate and test 15 for a belted trunk
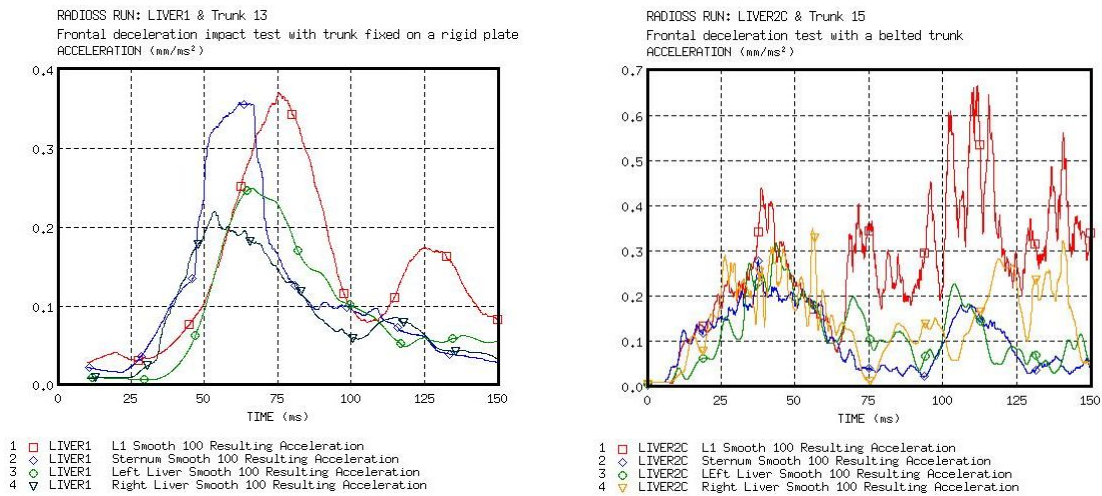
Figure 12: Resulting smoothed (100) acceleration curves for Test 13 with trunk on a rigid plate and test 15 for a belted trunk
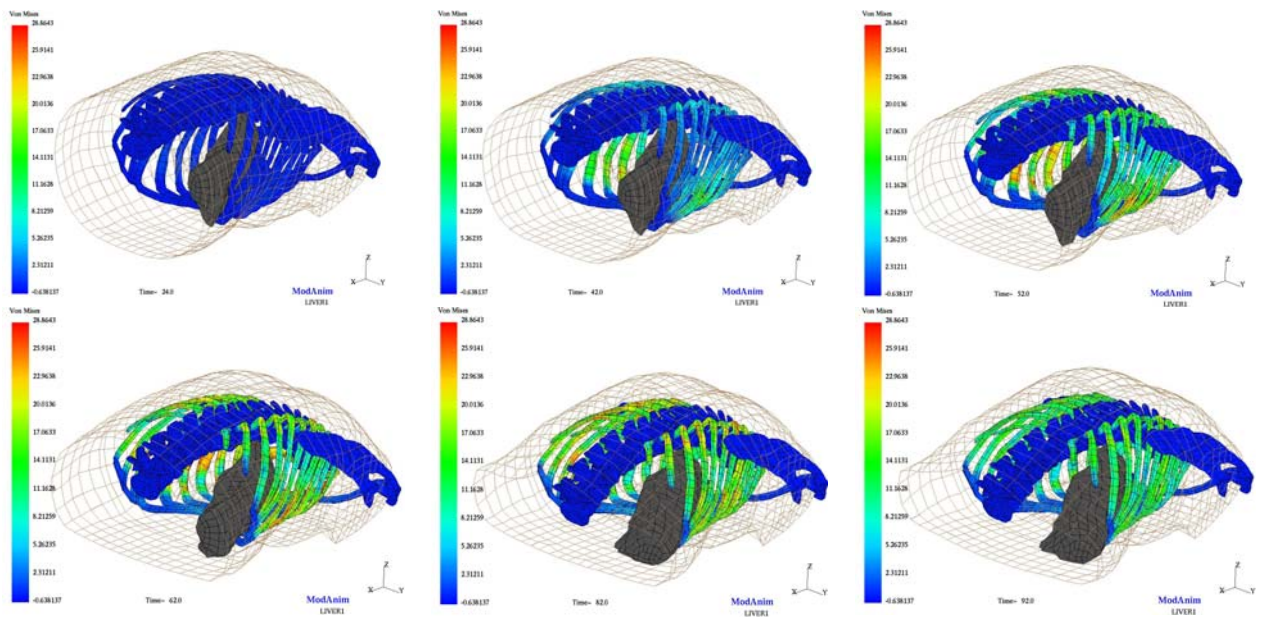
Figure n° 13 : Overview of Von Mises curves evolution on bones and cartilages for the trunk fixed on a rigid plate test
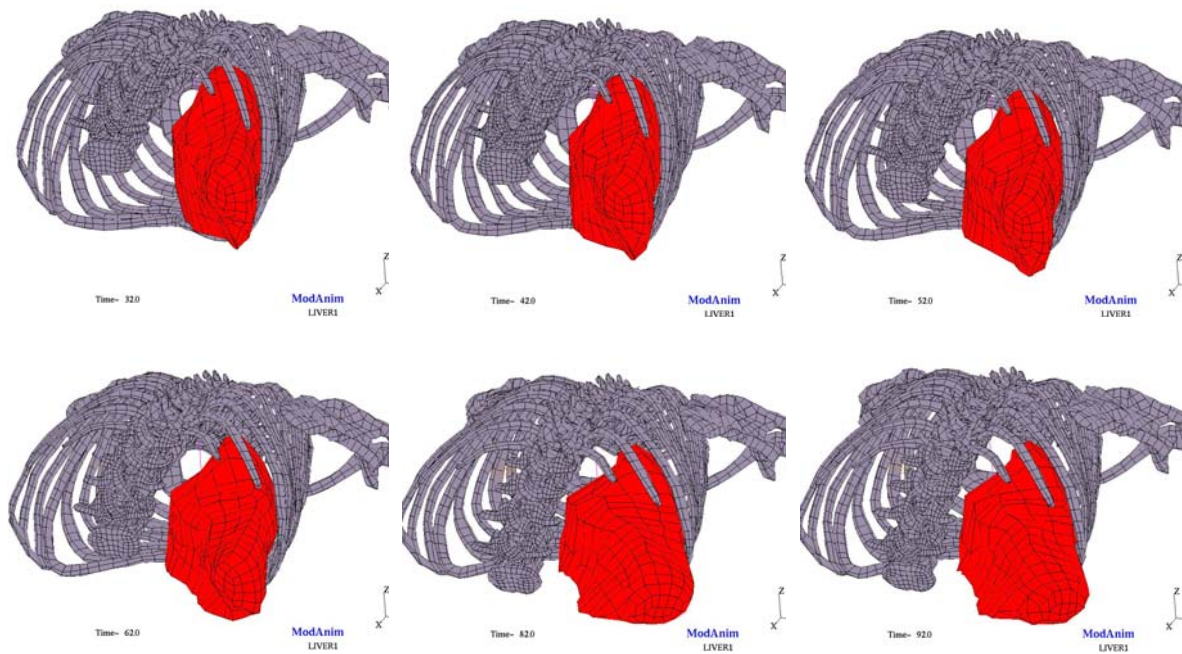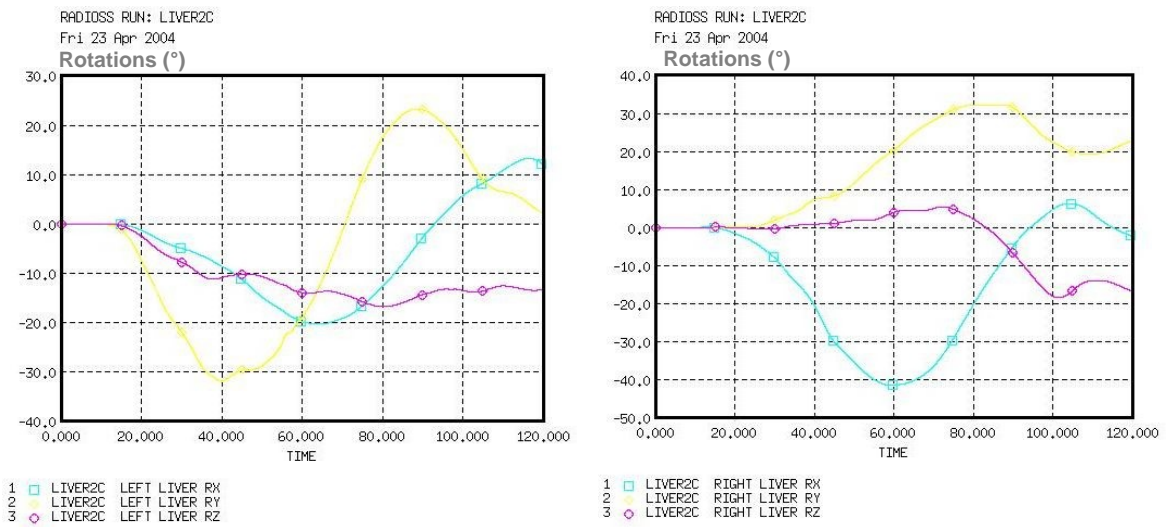

Figure 14: Rotation effects of the liver

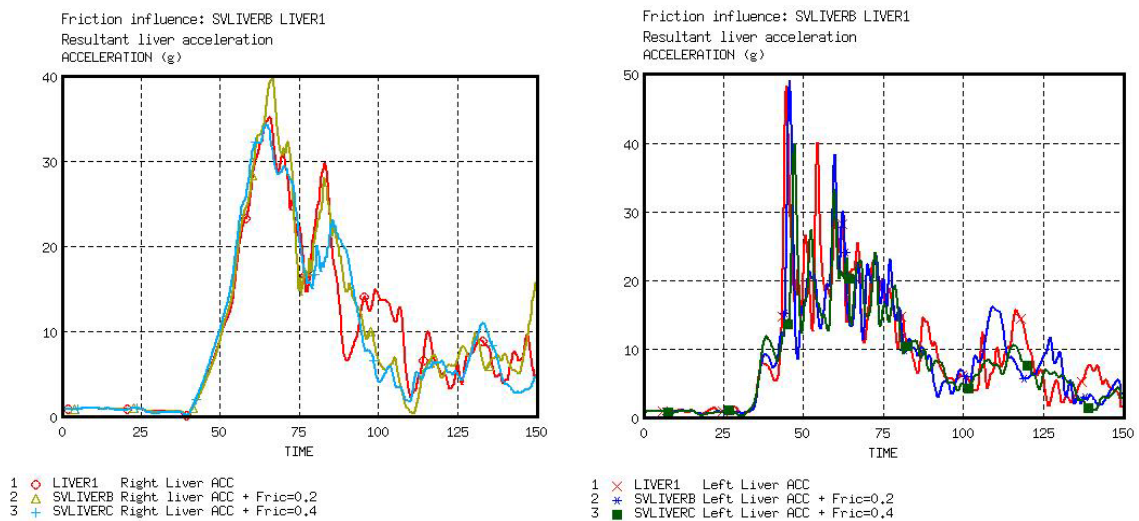**Figure 15:** Rotation effects (in degrees) versus Time (ms) of the right and left sensors of the liver

Figure 16: Comparison of Right and Left Liver resultant acceleration for reference test, 0,2 friction coefficient and 0,4 friction coefficient for all abdominal interfaces.
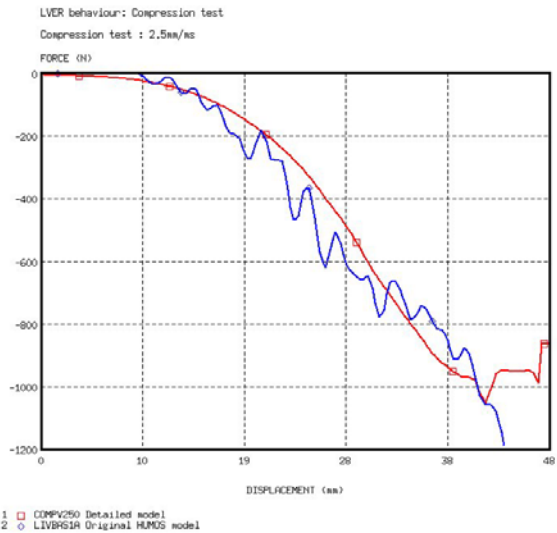
Figure 17: Illustration of the two compression tests performed with original HUMOS liver and a new liver model (tetra mesh with 1mm characteristic length compared to 10mm in Humos). The simulations consists to compression test with constant velocity of 2.5mm/ms
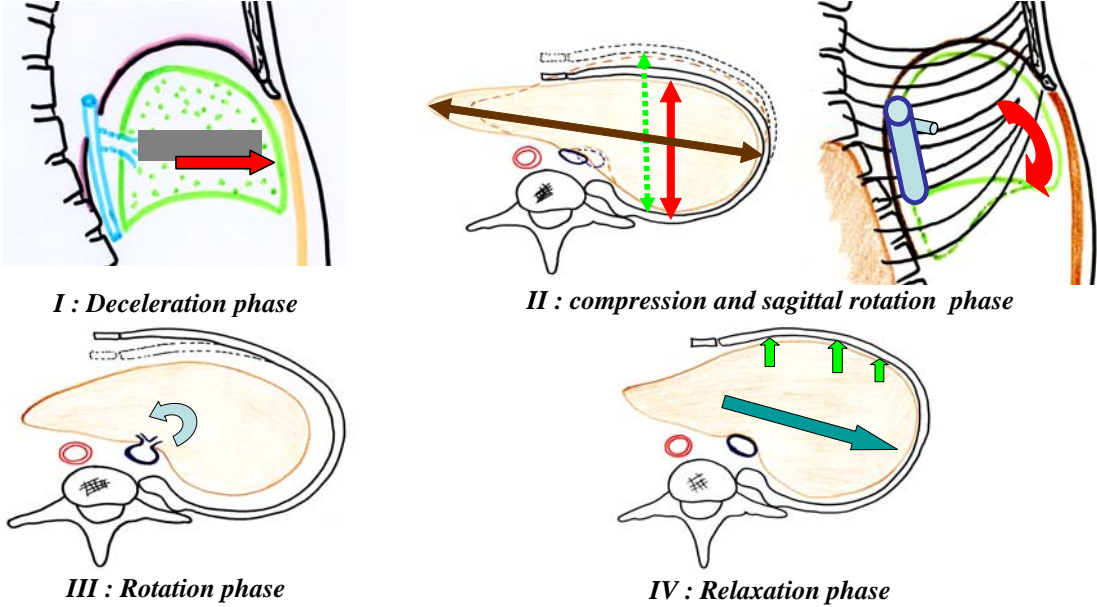

I : Deceleration phase

II : compression and sagittal rotation phase

III : Rotation phase

IV : Relaxation phase

Figure 18: Illustration of the three phase of the liver kinematics during the frontal deceleration in the transverse plan
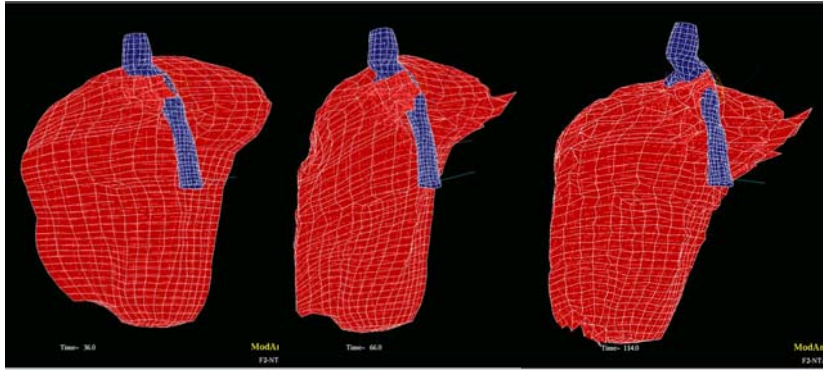
Figure 19: Illustration of the vein hepatic avulsion during torsion mechanisms of the liver for higher impact situation as performed in the current work